crystals

MDPI

Article

The Effect of 147 MeV ^{84}Kr and 24.5 MeV ^{14}N Ions Irradiation on the Optical Absorption, Luminescence, Raman Spectra and Surface of BaFBr Crystals

Abdirash Akilbekov [1], Daurzhan Kenbayev [1,2], Alma Dauletbekova [1,*], Alexey Shalaev [3], Aiman Akylbekova [1], Gulnara Aralbayeva [1], Zein Baimukhanov [1], Muratbek Baizhumanov [1], Edgars Elsts [4] and Anatoli I. Popov [4]

[1] Department of Technical Physics, L.N. Gumilyov Eurasian National University, 010008 Astana, Kazakhstan; akilbekov_at@enu.kz (A.A.); daurzhankenbayev@gmail.com (D.K.); aiman88_88@mail.ru (A.A.); agm_555@mail.ru (G.A.); zeinb77@mail.ru (Z.B.), zharast@gmail.com (M.B.)
[2] Department of Physical-Mathematical Sciences and Informatics, Shakarim University of Semey, 071412 Semey, Kazakhstan
[3] Vinogradov Institute of Geochemistry SB RAS, 664033 Irkutsk, Russia; alshal@igc.irk.ru
[4] Institute of Solid State Physics, University of Latvia, LV-1063 Riga, Latvia; edgars.elsts@cfi.lu.lv (E.E.)
* Correspondence: alma_dauletbek@mail.ru

Abstract: Today, BaFBr crystals activated by europium ions are used as detectors that store absorbed energy in metastable centers. In these materials, the image created by X-ray irradiation remains stable in the dark for long periods at room temperature. As a result, memory image plates are created, and they are extended to other types of ionizing radiation as well. Despite significant progress towards X-ray storage and readout of information, the mechanisms of these processes have not been fully identified to date, which has hindered the efficiency of this class of phosphors. In this study, using photoluminescence (PL), optical absorption (OA), Raman spectroscopy (RS), and atomic force microscopy (AFM), the luminescence of oxygen vacancy defects to BaFBr crystals irradiated with 147 MeV ^{84}Kr and 24.5 MeV ^{14}N ions at 300 K to fluences (10^{10}–10^{14}) ion/cm^2 was investigated. BaFBr crystals were grown by the Shteber method on a special device. Energy-dispersive X-ray spectroscopy (EDX) analysis revealed the presence of Ba, Br, F, and O. The effect of oxygen impurities present in the studied crystals was considered. The analysis of the complex PL band, depending on the fluence and type of ions, showed the formation of three types of oxygen vacancy defects. Macrodefects (tracks) and aggregates significantly influence the luminescence of oxygen vacancy defects. The creation of hillocks and tracks in BaFBr crystals irradiated with 147 MeV ^{84}Kr ions is shown for the first time. Raman spectra analysis confirmed that BaFBr crystals were amorphized by 147 MeV ^{84}Kr ions due to track overlap, in contrast to samples irradiated with 24.5 MeV ^{14}N ions. Raman and absorption spectra demonstrated the formation of hole and electron aggregate centers upon swift heavy ions irradiation.

Keywords: BaFBr; swift heavy ions; oxygen impurity; oxygen-vacancy defects; photoluminescence; track

Citation: Akilbekov, A.; Kenbayev, D.; Dauletbekova, A.; Shalaev, A.; Akylbekova, A.; Aralbayeva, G.; Baimukhanov, Z.; Baizhumanov, M.; Elsts, E.; Popov, A.I. The Effect of 147 MeV ^{84}Kr and 24.5 MeV ^{14}N Ions Irradiation on the Optical Absorption, Luminescence, Raman Spectra and Surface of BaFBr Crystals. *Crystals* **2024**, *14*, 480. https://doi.org/10.3390/cryst14060480

Received: 19 April 2024
Revised: 9 May 2024
Accepted: 16 May 2024
Published: 21 May 2024

1. Introduction

Barium fluorobromide with europium impurities, known as BaFBr:Eu^{2+}, has been widely used as an X-ray-preserving phosphor since it was first proposed for commercial use in 1983 [1]. The image created by X-rays in this material remained stable in the dark for a long time at room temperature. This property of phosphors is widely used for manufacturing X-ray memory imaging plates (IP) in medicine, biology, and physics [2–8]. In the field of medicine, the use of IP significantly reduces radiation exposure in patients during X-ray diagnostics. The dynamic range for image formation of IP based on BaFBr:Eu^{2+} exceeds five orders of magnitude, which is significantly higher than that of conventional X-ray films.

Initially developed for X-rays, imaging plates are now used for other types of ionizing radiation, such as neutrons, gamma rays, electron beams, protons, and ions. These materials have several important applications in various areas of radiation imaging. By including certain components (Gd_2O_3 or ^6LiF) in BaFBr:Eu^{2+}, thermal neutron detectors (NIP) and neutron image plates have been developed [9–12]. The possibility of registering heavy-ion microbeams using BaFBr:Eu^{2+} was considered [13], and the behavior of the imaging plate under heavy-ion irradiation was examined in a previous study [14].

Alkaline earth metal fluorohalides MeFX (Me–Ca, Sr, Ba and X–Cl, Br, I) crystallize in the tetragonal structure of the PbFCl type with the space group P4/nmm [15]. In [16], the crystal structures of BaFBr crystals were determined. These compounds are mixed single crystals of layered alkaline earth halogens. As a result of these studies, it was found that there are two types of anionic nodes in the structure of these crystals: two types of anionic vacancies, $\alpha(F^-)$- and $\alpha(Br^-)$- centers, and two types of F centers, $F(F^-)$- and $F(Br^-)$-centers. These centers have C_{4v} and D_{2d} symmetry, and their optical characteristics are well established; however, other types of hole defects are practically unexplored, except for those formed at low temperatures, such as self-trapped holes or V_k-centers [17–28]. It should be noted that the presence of a TSL peak at 363 K complicates the study of defects caused by rapid bleaching [27]. Radiation defects play an important role in the luminescence and memory mechanisms of the BaFBr:Eu^{2+} phosphors. However, the exact mechanism of these processes is still not clear, which inhibits the increase in luminophore efficiency and leaves the fundamental problem of defect interactions in this phosphor unresolved.

For commercial use, BaFBr:Eu^{2+} is applied in the form of powder on a transparent base to create X-ray screens. These image plates are used in both commercial and research settings. However, the characteristics measured are not enough to provide a complete understanding of the luminescence centers and their role in the creation, conversion, and photostimulated emission luminescence mechanisms. To study these aspects in more detail, single-crystal samples are needed so that absorption and luminescence spectroscopy techniques can be applied to crystals in their entirety. It is therefore important to investigate the behavior of oxygen impurities in a single crystal, especially for comparative experiments.

The aim of our study was to investigate stable radiation defects in BaFBr single crystals with uncontrolled oxygen impurities. Oxygen impurities are the most typical impurities in these crystals, but their influence is not so obvious. BaFBr crystals were irradiated with swift heavy ions (SHI) 147 MeV ^{84}Kr ions, and 24.5 ^{14}N ions at different fluences at 300 K, and investigated using photoluminescence (PL), absorption spectroscopy, atomic force microscopy (AFM), and Raman spectroscopy (RS).

2. Materials and Methods

BaFBr:Eu^{2+} material is widely used as a memory phosphor. This means that it can preserve the image created by X-rays in the dark for a long time at room temperature. For commercial use, BaFBr:Eu^{2+} is applied in the form of powder on a transparent base to create X-ray screens. These screens are used for both commercial and research purposes. However, the characteristics measured for such screens are insufficient to obtain complete information on the structure of the luminescence centers and their role in the mechanisms of radiation creation, transformation, and photostimulated luminescence. To study these aspects, single-crystalline samples are required to apply the methods of absorption and luminescent spectroscopy of crystals in their entirety.

BaFBr is a crystal that belongs to tetragonal symmetry and crystallizes in the structural type PbFCl. The crystals have good cleavage with layers perpendicular to the *z*-axis. After analyzing the literature [29–31], it was established that the Bridgman–Stockbarger method is commonly used for the growth of BaFBr single crystals. The melting temperature of BaFBr ranges from 989 to 1070 °C. Methods of obtaining single crystals of BaFBr are similar to those of other crystals with a structure like PbFCl (BaFCl, BaFBr, BaFI, SrFCl, etc.) and differ only in minor details. The literature data [32–34] suggest that BaFBr single crystals grow at sufficiently high rates from their own melt (congruent melting). However, they

crack when exposed to sudden temperature jumps or when they enter a zone with a high temperature gradient. Considering these features during growth, and the fact that BaFBr has a relatively low melting temperature, it was decided that the Steber method would be used for the growth of BaFBr single crystals. The Steber method assumes the presence of "soft" thermal conditions and simplifies the growth process compared to the Bridgman–Stockbarger method. This eliminates the need to move the crucible and the need for special zones with different temperatures.

BaFBr crystals were grown by the Shteber method on a special device (Vinogradov Institute of Geochemistry SB RAS, Irkutsk, Russia). Graphite is the most commonly used material for manufacturing heating units and crucibles due to its thermal properties and interaction with melt BaFBr. The reducing ability of graphite is one of its most important properties in this regard. Another crucial property is the absence of wettability of graphite with barium fluorobromide melt.

This facilitates easy removal of the crystal from the crucible after its growth. The crucible, attached to a cooled rod with a special nozzle, rotates during the growth process while the heating unit maintains a temperature gradient of 4–6 degrees per centimeter.

The crystals were grown in a helium-fluoride atmosphere using stoichiometric mixtures of $BaBr_2$ and BaF_2. The starting material, $BaBg_2$ $2H_2O$, was subjected to vacuum drying at 500 °C.

Elemental analysis was performed by energy-dispersive X-ray spectroscopy (EDX) or (EDS) using an SEM Hitachi TM3030 (Hitachi High-Technologies Corporation, Tokyo, Japan) with a Bruker attachment and software quantax 70 (Bruker Nano GmbH, Berlin, Germany). EDX analysis. EDX is a method used to identify the composition of solid materials. This technique relies on exciting electrons close to the nucleus, which then causes distant electrons to lower their energy levels to fill the resulting holes. Each element releases a different set of X-ray frequencies when filling these holes, which can provide both qualitative and quantitative information about the near-surface composition of a sample. The data in Table 1 demonstrate that BaFBr crystals are stoichiometric, but they also contain some oxygen impurities. Carbon particles with a peak of 0.3 keV were not considered because of the presence of carbon in the chamber.

Table 1. The elemental composition of the samples.

Element	F	Br	Ba	O
Atomic percent	38.3	32.9	25.2	3.6

BaFBr crystal samples were irradiated with 147 MeV ^{84}Kr and 24.5 MeV ^{14}N ions at 300 K to fluences (10^{10}–10^{14}) ion/cm^2 at accelerator DC-60 (Astana, Kazakhstan). The radiation parameters of 147 MeV ^{84}Kr and 24.5 Mev ^{14}N ions in the BaFBr crystal were obtained using the SRIM code [35] and are summarized in Table 2.

Table 2. Radiation parameters of 147 MeV ^{84}Kr and 24.5 Mev ^{14}N ions in the BaFBr crystal.

Ion	Energy, Mev	S_e, keV/nm	S_n, keV/nm	R, μm
^{84}Kr	147	12.04	1.36	17.87
^{14}N	24.5	2.99	0.00258	15.58

S_e denotes the ionization losses, S_n represents the elastic collision losses, and R is the range of ions.

The ratio (S_e/S_n) = 8.8 for the 147 MeV ^{84}Kr ion and 1159 for the 24.5 MeV ^{14}N ion. Electron losses dominate for nitrogen ions; in the case of krypton, it is necessary to consider both ionization losses and elastic collision losses.

The PL spectra of the crystals were measured according to the standard procedure using an SM2203 spectral fluorimeter (SOLAR, Minsk, Belarus). In this device, the excitation

source was a xenon FX-4401 flash lamp (PerkinElmer Optoelectronics GmbH, Wiesbaden, Germany) with a pulse duration of a few microseconds, and the light detector was PMT R928 (Hamamatsu, Japan). The control of the device and processing of the results of measurements are carried out from the external computer by means of the "Universal" (SOLAR, Minsk, Belarus) software.

Optical absorption spectra were measured using a Specord UV-VIS spectrophotometer (SPECORD 250 PLUS, Jena, Germany) in the spectral interval (2.0–6.0) eV. This is a double-beam spectrophotometer with variable spectral bandwidth and a double monochromator, in which the wavelength setting accuracy is ±0.1 nm. An external personal computer using WinASPECT software was used to control the device and process data during measurements.

Raman spectra were measured at room temperature with a Solver Spectrum spectrometer (NT-MDT America Inc., Tempe, AZ 85283, USA) using a solid-state diode laser beam with a wavelength of 473 nm (2.62 eV) and a spectral resolution of 1 cm^{-1}. The laser was focused using a 100× objective to form a spot on the sample surface with a diameter of 2 μm.

The surface morphology of unirradiated and ion beam irradiated BaFBr samples was investigated by atomic force microscopy using an AIST-NT SmartSPM microscope (AIST-NT, Moscow, Russia) at scan sizes of 30 μm × 30 μm.

3. Results and Discussion

In stoichiometric BaFBr single crystals and X-ray image plates, oxygen plays an important role in the creation of electron and hole centers [36]. There are two known types of oxygen centers in BaFBr: O_{Br}^{-} centers (where an O^{-} ion takes the place of bromine Type II) and O_{F}^{-} centers (where an O^{-} ion takes the place of fluorine, Type I) [37,38]. Two more oxygen centers were later found in [39,40]. One of these centers has the same structure and symmetry as the known O_{Br}^{-} center but has different hyperfine interaction constants, which can be labeled as (Type IIA). The second oxygen center consists of an oxygen molecular ion O_{2}^{-} with one atom at the bromine site and one atom at the neighboring fluorine site.

Sensitive to impurity defects is the photoluminescence method, which we applied to study oxygen vacancy defects. PL spectra of BaFBr crystals irradiated with 147 MeV ^{84}Kr and 24.5 MeV ^{14}N ions excited with 280 nm wavelength light are shown in Figure 1. The spectra were measured after a sufficiently long exposure of the irradiated crystals at room temperature in the dark.

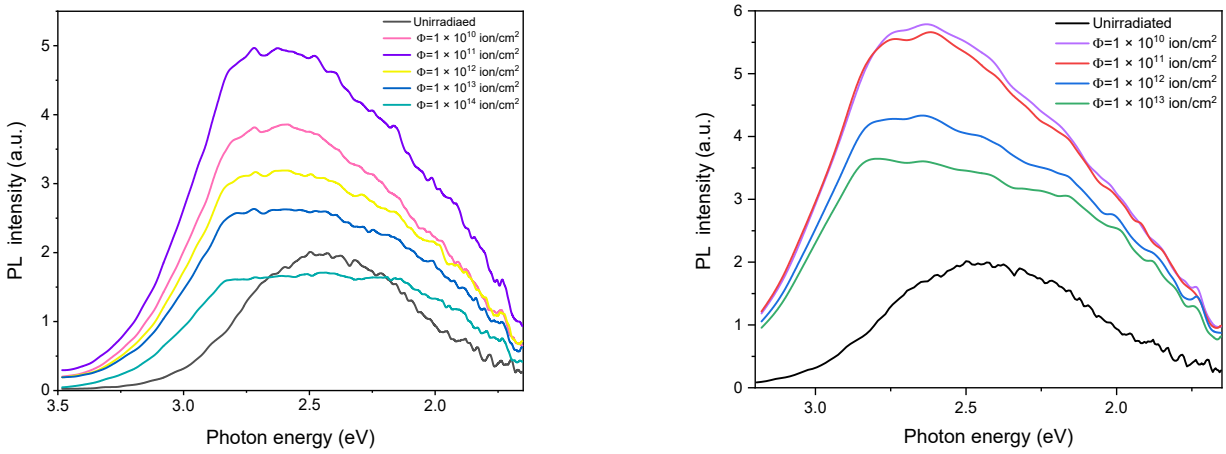

(**a**) (**b**)

Figure 1. (**a**) PL spectra of BaFBr crystals irradiated by 147 MeV ^{84}Kr ions via fluence; (**b**) PL irradiated by 24.5 MeV ^{14}N ions via fluence. The fluencies (1 × 10^{10}–1 × 10^{14}) ion/cm^2. Exiting light with λ = 280 nm (4.43 eV), T = 300 K.

The PL spectra of the unirradiated and irradiated samples were mainly characterized by a complex luminescence band ranging between 1.75 and 3.5 eV. This band can be decomposed into two bands with peaks at 2.5 eV and 2.05 eV, which correspond to oxygen vacancy defects (Type I) with a maximum of 2.5 eV and (Type II) with a maximum of 2.05 eV [41]. The absorption bands of the centers are shown in Figure 2.

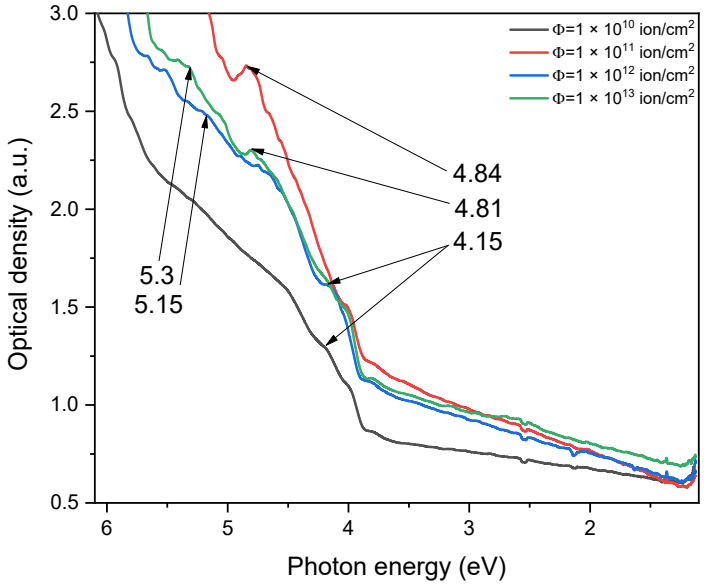

Figure 2. Absorption spectra of BaFBr irradiated with ions 24.5 MeV ^{14}N at RT via fluence. Fluence range (1×10^{10} ion/cm^2–1×10^{13}) ion/cm^2.

Absorption bands with maxima 7.0 eV, 6.3 eV, and 4.95 eV for centers (Type I) [41]. In our experiment, the band 4.95 eV was established; the other two were not measured due to the limited spectral range of the spectrophotometer. The center (Type II) corresponds to the absorption bands at 4.15 eV and 5.3 eV, which is consistent with the absorption band maxima of 6.35 eV, 5.28 eV, and 4.2 eV by [41].

The center (Type I) in stoichiometric BaFBr crystals consists of an oxygen ion replacing the fluorine ion and a neighboring v_{Br}^{+} vacancy compensating for the charge. Then the model of this center is represented as O_F^{-}–v_{Br}^{+}; see Figure 3a. In the second type center, the oxygen ion replaces the bromine ion and is located next to the bromine vacancy. The design of this center resembles the following: O_{Br}^{-}–v_{Br}^{+}; see Figure 3b.

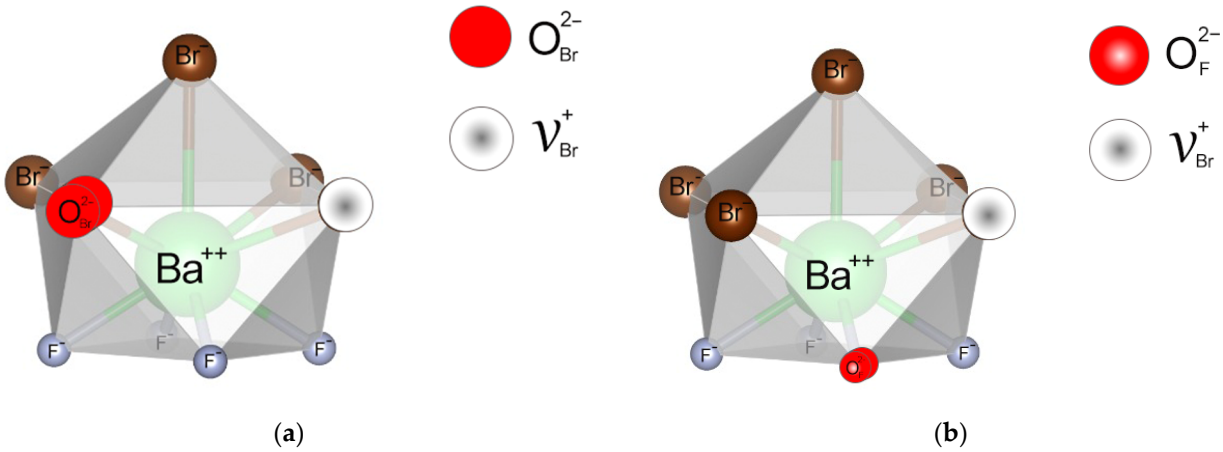

(**a**) (**b**)

Figure 3. (**a**) Model of the defect O_F^{2-}–v_{Br}^{+}. (**b**) Model of the defect O_{Br}^{2-}–v_{Br}^{+}.

Both types of centers were present in the unirradiated crystal, Figures 1 and 2, indicating the incorporation of oxygen ions into the lattice during growth. Upon irradiation with 147 MeV ^{84}Kr ions, a linear increase in the luminescence intensity of both centers was observed up to a fluence of 10^{11} ions/cm^2, as shown in Figures 1 and 4. A further increase in dose led to saturation and a decrease in luminescence intensity. Upon irradiation with 24.5 MeV ^{14}N ions, a linear increase in the luminescence intensity of both types of defects was observed. At a fluence of 10^{12} ions/cm^2, after saturation, the intensity began to decrease, as shown in Figures 1 and 4. Thus, along with the existing oxygen, vacancy defects, the mechanism for creating these defects during irradiation by SHI was investigated. It should be noted that the luminescence intensity of the crystals exposed to nitrogen ions was higher than that of the crystals irradiated with krypton ions (Figures 1 and 4). Similar behavior of the 390 nm (3.18 eV) luminescence band was observed for BaFBr: Eu^{2+} irradiated BTI (^{22}Ne, ^{52}Cr, ^{64}Zn, ^{130}Xe, and ^{238}U) [14]. In this study, samples prepared by homogenizing BaFBr powders with 0.1 mol% Eu^{2+} together with polyester and cellulose ether FX-225 binders were used. The granules that were acquired were placed onto the PET substrate. The 390 luminescence band is due to (F(F^-), F_A(Eu^{2+}, F^-), and F(Br^-)) centers, according to the authors. At low doses, the PL intensity shows a linear dependence. Then saturation occurs, and a further increase in fluence leads to a decrease in PL. The dependence on ion type, dose, and energy loss was established. The authors attribute the decrease in intensity to the creation of macrodefects and draw an analogy with BaF_2, in which the threshold value of S_e = 7 keV/nm under SHI irradiation. This condition is true for Cr and U ions.

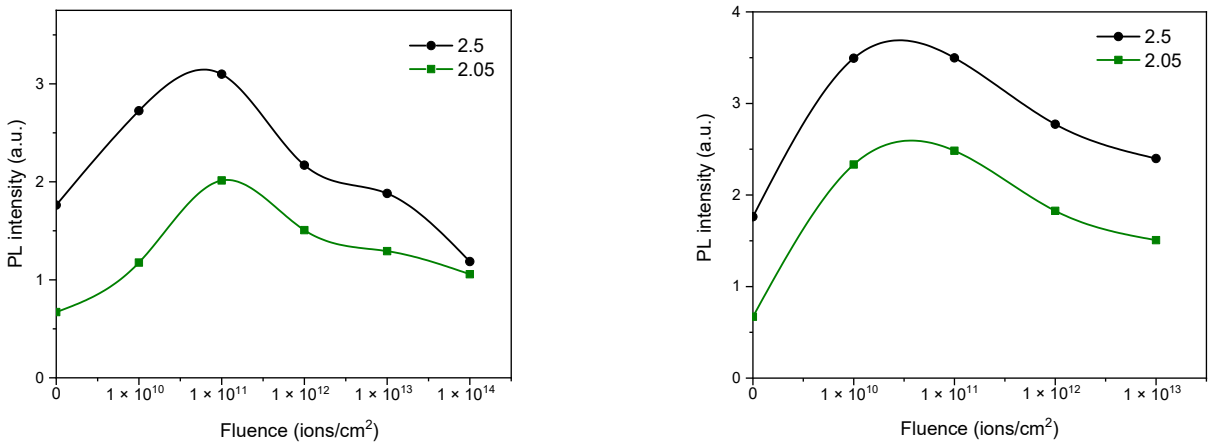

Figure 4. Dependence of luminescence intensity of oxygen vacancy defects of two types (2.5 eV and 2.05 eV) on fluence: (**a**) for crystals irradiated by 147 MeV ^{84}Kr ions, and (**b**) for crystals irradiated by 24.5 MeV ^{14}N ions.

Thus, the decrease in oxygen vacancy defects luminescence intensity can be explained by reabsorption in the irradiated layer and scattering on macrodefects (hillocks, tracks), aggregates produced by irradiation with 147 MeV ^{84}Kr ions S_e = 12.04 keV/nm, and aggregate defects in crystals irradiated by 24.5 MeV ^{14}N ions because S_e = 2.99 keV/nm.

Initially, the crystals have a fairly close correlation between the centers, but irradiation leads to a more efficient creation of bromine vacancies because the number of bromine vacancies in these two centers is 3:1. According to [41], the luminescence of Type II center should be between the luminescence of the centers of Type I and Type II. This process most likely led to a shift in the luminescence band peak. This effect was more pronounced when irradiated with nitrogen ions. Irradiation with 24.5 Mev ^{14}N leads to defect formation due to the creation of electronic excitations (e^-, h, e^--h, e^0). Similar to AHC (Alcaly Halide Crystals), the decay of autolocalized excitons, similar to AHC, results in the generation of

Frenkel pairs (F-H, α-I) of defects and aggregates. The work [14,42] explains how radiation defects are created in $BaFBriEu^{2+}$, using AHC as an analogy.

This is due to the dominance of electron energy losses in BaFBr crystals when irradiated with nitrogen ions compared to krypton ions. The Gaussian decomposition of the PL curves corresponding to the largest shear is shown in Figure 5.

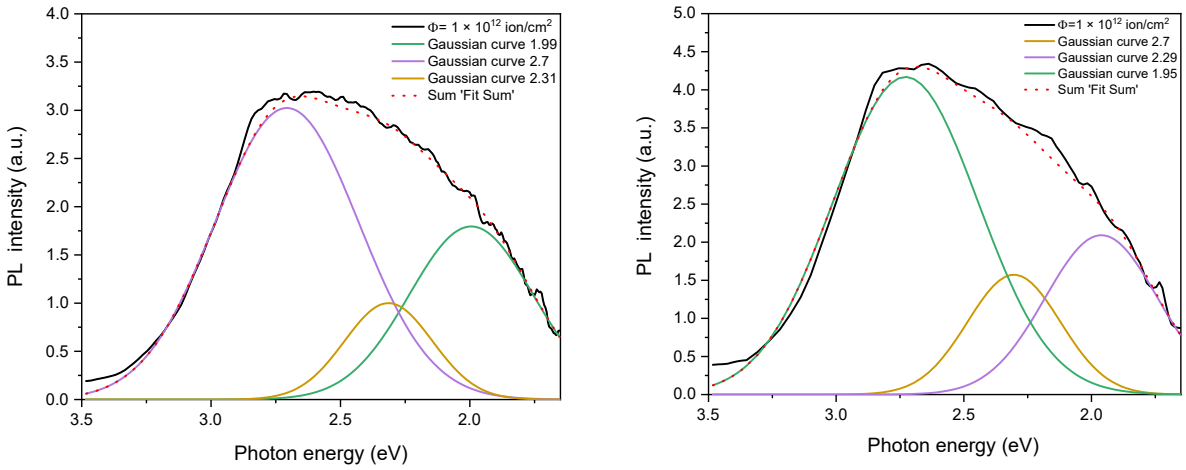

Figure 5. Gauss components of PL spectra of BaFBr crystals irradiated by ions: (**a**) ^{84}Kr 147 MeV $\Phi = 1 \times 10^{12}$ ions/cm^2; (**b**) ^{14}N 24.5 MeV $\Phi = 1 \times 10^{12}$ ion/cm^2.

It is assumed that the $O_F^- – v_F^+$ center (Type III) [41] corresponds to luminescence with a maximum of 2.31–2.29 eV. Accordingly, the PL band of the first center shifts to 2.7 eV, and the PL band of the second center shifts to the 1.95–1.99 eV position. Furthermore, it should be noted that various other types of oxygen vacancy defects, which were previously mentioned, will also have an impact.

As mentioned earlier, the decrease in luminescence can be explained by reabsorption in the irradiated layer and by scattering on macrodefects (hillocks and tracks), as shown in Figure 6, and aggregates. Tracks were created in BaFBr crystals irradiated with 147 MeV ^{84}Kr ions. A larger decrease in PL intensity was observed for these crystals, as shown in Figure 1a.

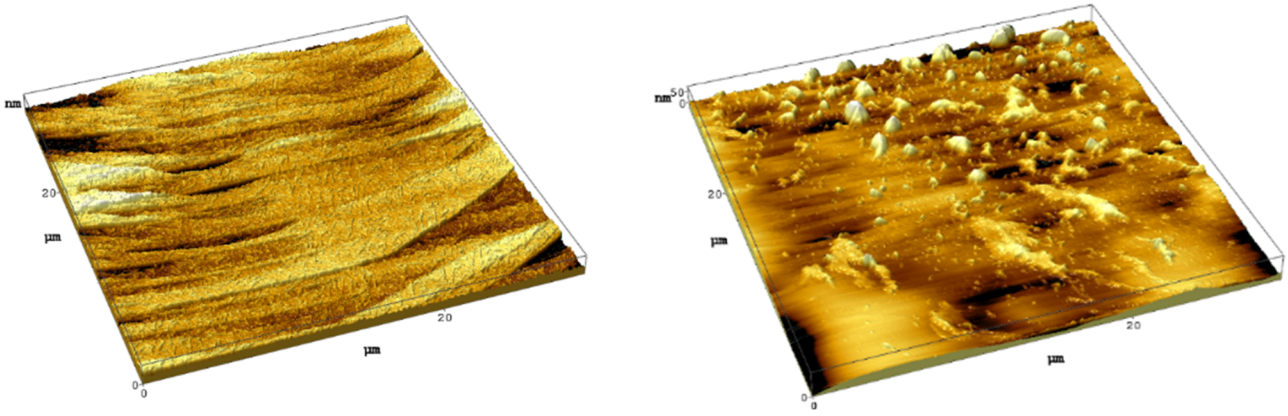

Figure 6. AFM 3D images of BaFBr: (**a**) unirradiated, and (**b**) irradiated by 147 MeV ^{84}Kr ions to fluence 10^{11} ions/cm^2.

Tracks in the form of extended disordered regions were first recorded after the chemical treatment of dielectric solid-state detectors irradiated with fission fragments [43]. Later,

after irradiation with high-energy ions, it was found that tracks appeared starting from a certain threshold level of electronic energy loss S_e. Electronic energy losses of S_e with radial energy distribution are the first stage of any consideration of tracks [44].

Let us continue the analogy with AHC. According to [45], the track consists of a central part, the "core", or nucleus, with a radius of a few nm, an intermediate region (radius up to 10 nm), and a wide cylindrical halo whose size depends on the parameters of the attacking ion. The track halo contains predominantly F centers. The intermediate region is distinguished as a separate part of the track, detected starting from the Se ~5 keV/nm electron loss threshold by the increased radiation-induced volume. After being irradiated by ions with S_e above the critical S_e (approximately 6 keV/nm), hillocks are formed on the surfaces of many dielectrics. These hillocks have been studied using AFM and SEM [46,47]. We can indeed see the formation of hillocks on the surface of BaFBr; see Figure 6b. To date, it has been established by HP TEM (high-resolution transmission electron microscopy) that exposure to single high-energy ions leads to the formation of crystalline hillocks on the surface of TiO_2 [48], CeO_2, AHC, CaF_2, SrF_2, BaF_2, and amorphous hillocks on the surface of iron yttrium garnet YIG [49]. Hillocks may contribute to decreased luminescence intensity, particularly with increasing fluence, due to light scattering.

Significant amorphization of BaFBr crystals irradiated with high-energy krypton ions was established by studying the Raman spectra.

The Raman spectra of crystals irradiated with 147 MeV ^{84}Kr ions as a function of fluence are shown in Figure 7a. The FWHM and main Raman modes [50–52] are analyzed in Table 3 and the insets of Figure 7a.

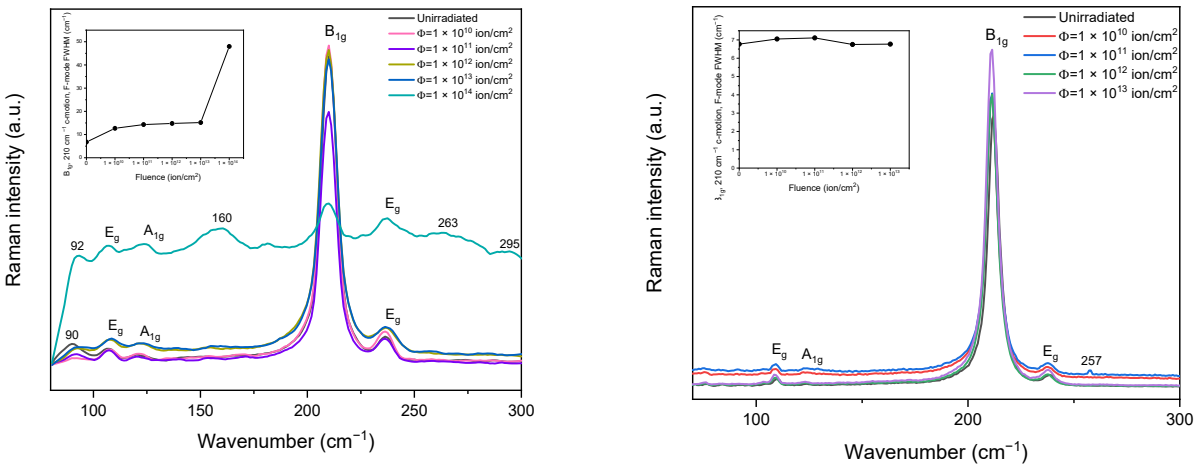

Figure 7. Raman spectra of BaFBr crystals irradiated with SHI via fluence: (**a**) ^{84}Kr 147 MeV; (**b**) 24.5 MeV ^{14}N. The insets show the FWHM of the main mode 210 cm^{-1} dependence as a function of fluence.

The main RS band at 210 cm^{-1} broadens with increasing fluence, which shows amorphization associated with the formation of tracks, and at a fluence of 10^{14} cm^{-2} at a high level of track overlapping, the spectrum degrades; see Figure 7a. There was no broadening of the band at 210 cm^{-1} for the nitrogen ion irradiation, as shown in Figure 7b.

Upon irradiation with nitrogen ions, aggregation of electron and hole color centers was observed, starting at a fluence of 10^{12} ions/cm^2. In [53], we compared the RSs of X-irradiated KBr [54] and BaFBr crystals to determine the part caused by V centers (hole aggregates). It consists of bands at 175 cm^{-1}, 265 cm^{-1}, and 349 cm^{-1}, where 265 cm^{-1} and 349 cm^{-1} are the first overtones of the 175 cm^{-1} mode. Figure 8 shows these bands for crystals irradiated with 147 MeV ^{84}Kr, Figure 8a, and 24.5 MeV ^{14}N ions, Figure 8b.

Table 3. The FWHM of Raman spectra bands dependence as a function of fluence for BaFBr crystals irradiated by ^{84}Kr 147 MeV and 24.5 MeV ^{14}N.

Fluence Φ, ion/cm^2	^{84}Kr 147 MeV FWHM, cm^{-1}			^{14}N 24.5 MeV FWHM, cm^{-1}		
	E_g, ab-Motion, Anti-Parallel, Br Mode	B_{1g}, c-Motion, F-Mode	E_g, ab-Motion, F-Mode	E_g, ab-Motion, Anti-Parallel, Br Mode	B_{1g}, c-Motion, F-Mode	E_g, Ab-Motion, F-Mode
Unirradiated	7.86	6.77	16.06	7.86	6.77	16.06
1×10^{10}	59.75	12.68	32.06	9.22	7.05	16.17
1×10^{11}	51.28	14.30	33.02	10.24	7.11	9.64
1×10^{12}	73.76	14.78	47.82	8.03	6.75	10.08
1×10^{13}	79.10	15.18	49.63	7.24	6.77	10.78
1×10^{14}	87.66	47.96	115.91	-	-	-

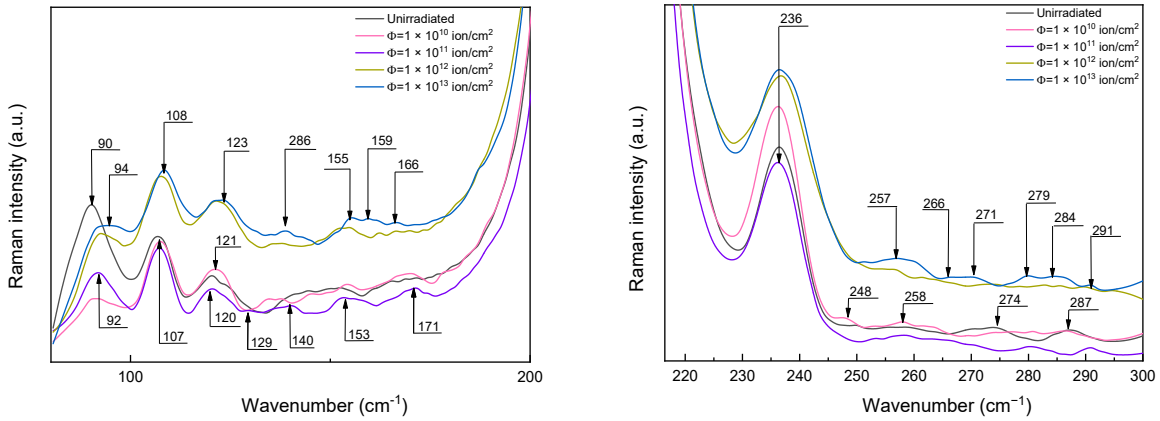

(**a**)

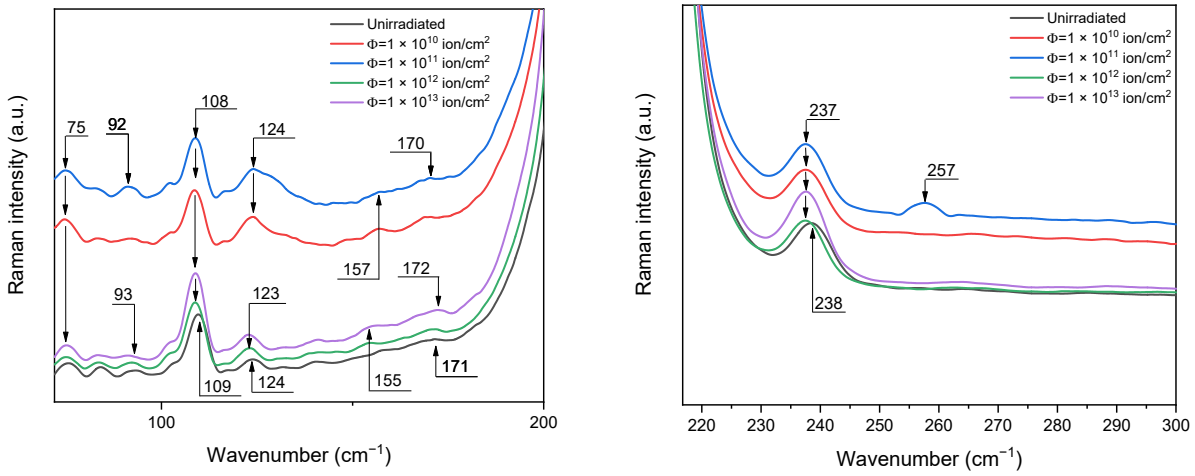

(**b**)

Figure 8. Raman spectra of BaFBr as a function of fluence: (**a**) with 147 MeV ^{84}Kr ions; (**b**) with 24.5 MeV ^{14}N ions.

These modes correspond to the V center (hole aggregates) in KBr crystals irradiated with X-rays [55]. As shown in Figure 8, the SHI-irradiated BaFBr crystals exhibit similar cen-

ters. Aggregation began at a fluence of 10^{11} ions/cm^2 for 147 MeV, ^{84}Kr, and 10^{12} ions/cm^2 for 24.5 MeV ^{14}N ions. The aggregation of complementary electron centers exhibited a similar pattern. Figure 9 displays the absorption spectrum of the M centers, which are aggregates of two F centers.

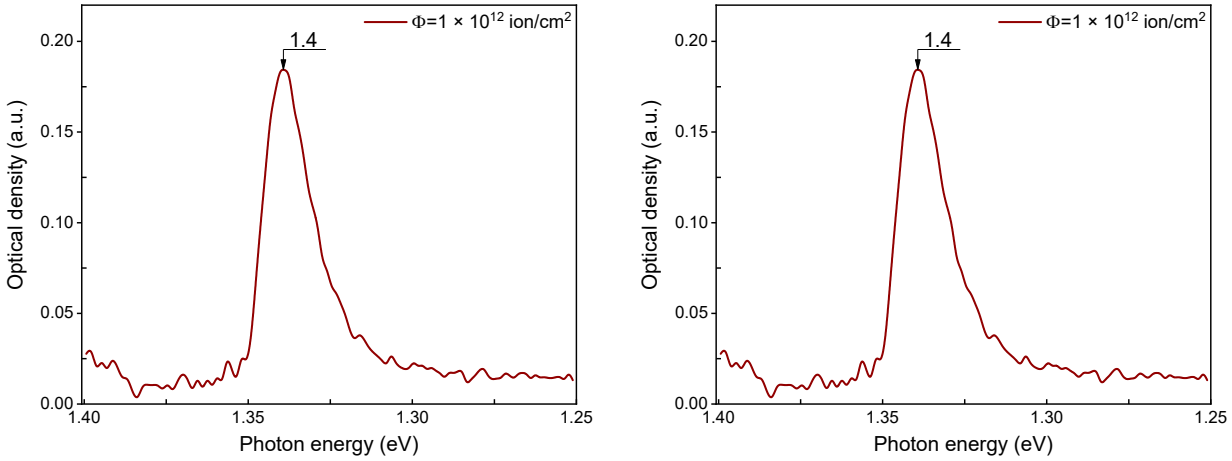

Figure 9. The absorption spectrum of BaFBr crystal irradiated with: (**a**) 147 MeV Kr ions; (**b**) 24.5 MeV N ions, to a fluence of 10^{12} ion/cm^2.

It should be noted, neither at room temperature nor at helium temperature were H centers detected. It is possible that H centers are not stable at room temperature. We indirectly demonstrate the creation of H centers through the formation of hole aggregates—V centers. When an ionizing particle or quantum enters the crystal, it generates low-energy electronic excitations such as electron–hole pairs and excitons. Impurity defects can capture electrons and holes. Self-trapped excitons can decay radiationless with the creation of Frenkel pair (F-H) centers. That is, the energy released during exciton decay moves the bromine atom from its regular position in the interstitium, leaving an electron, which together with the anion vacancy formed in this case, constitutes the F(Br^-)-center. A bromine atom displaced to the internode combines with a nearby bromine ion to form the H-center (Br_2^- center). Such an H center diffusing through the lattice, relaxes with a nearby Eu^{2+} ion, forming the so-called Eu^{2+}/H luminescent complex. Such a luminescent complex plays the role of a recombination center in the process of photostimulated luminescence. On the other hand, it is assumed that at room temperature, impurity oxygen ions serve as extra hole traps, which further aid in the creation of F centers. According to the authors, this method of forming electron–hole–electron centers is even more likely than the typical formation of F-H pairs, which is suggested in reference [56]. Our studies show that SHI-irradiated BaFBr crystals can perform these two processes.

4. Conclusions

For the studied BaFBr crystals irradiated with 147 MeV ^{84}Kr and 24.5 MeV ^{14}N ions and stored for a long time in the dark, oxygen impurities were observed. So, a band from 1.5 eV to 3.5 eV was observed in the PL spectrum, which is also present in the unirradiated crystal but with a lower intensity and is associated with oxygen impurities. The complex PL band includes the luminescence of the main two oxygen vacancy centers with different structures. In unirradiated crystals, the luminescence of oxygen vacancy centers with a maximum of 2.5 eV dominates. This indicates that oxygen is mostly present at the regular bromine site. When the fluence was increased to 10^{11} ion/cm^2, there was an increase in the luminescence intensity of the first type (2.5 eV), second type (2.05 eV), and third (2.3 eV) centers. The creation of the third type results in a shift in the maximum of the other two

types of centers. It was discovered that oxygen vacancy centers are formed not only during crystal growth but also through the process of SHI irradiation.

Macrodefects (hillocks and tracks) and aggregates significantly influence the luminescence of oxygen—vacancy defects. The creation of hillocks and tracks in BaFBr crystals irradiated with 147 MeV ^{84}Kr ions is shown for the first time. Hillocks may contribute to decreased luminescence intensity, particularly with increasing fluence, due to light scattering. Significant amorphization of BaFBr crystals irradiated with high-energy krypton ions was established by studying Raman spectra.

Raman spectra analysis confirmed that BaFBr crystals were amorphized by 147 MeV ^{84}Kr ions due to track overlap, in contrast to samples irradiated with 24.5 MeV ^{14}N ions. Raman and absorption spectra demonstrated the formation of hole and electron aggregate centers upon SHI irradiation.

The PL effects in ion-irradiated BaFBr single crystals are seen to be closely related to the damage creation in the BaFBr matrix.

The results obtained expand the range of ideas about oxygen vacancy effects in BaFBr crystals. The results on track formation are promising. Here, the main research direction can be related to the layered structure of crystals and track behavior.

Author Contributions: Conceptualization, A.I.P. and A.A. (Abdirash Akilbekov); methodology, A.D. and D.K.; software, G.A.; validation, A.D., D.K. and A.S.; formal analysis, A.I.P. and A.S.; investigation, D.K., G.A., Z.B., E.E., A.A. (Aiman Akylbekova) and M.B.; data curation, D.K., G.A. and A.A. (Aiman Akylbekova); writing—original draft preparation, A.D.; writing—review and editing, A.I.P. and A.A. (Abdirash Akilbekov); supervision, A.A. (Abdirash Akilbekov); project administration, A.D.; funding acquisition, A.A. (Abdirash Akilbekov). All authors have read and agreed to the published version of the manuscript.

Funding: This work was funded by the Ministry of Science and Higher Education of the Republic of Kazakhstan under grant number AP14870572.

Data Availability Statement: The raw data supporting the conclusions of this article will be made available by the authors on request.

Acknowledgments: We are grateful for the financial support provided by Grant No. AP14870572 from the Ministry of Science and Higher Education of the Republic of Kazakhstan. We also extend our thanks to I. Ivanov for irradiating the crystals at the DC-60 cyclotron.

Conflicts of Interest: The authors declare no conflicts of interest.

References

1. Sonada, M.; Takano, M.; Miyahara, J.; Kato, H. Computed radiography utilizing scanning laser stimulated luminescence. *Radiology* **1983**, *148*, 833–838. [CrossRef] [PubMed]
2. Gurvich, A.M.; Myakhkova, M.G.; Rudiger, J.; Kavtorova, V.P. Phosphors for conventional and computed radiography. *Nucl. Tracks Rad. Meas.* **1993**, *21*, 29–33. [CrossRef]
3. Rajan, K.G.; Yousuf, M.; Subramanian, N.; Pumiah, B.; Kasiviswanathan, K.V. Photostimulable luminescence: Physics and applications. *Indian J. Pure Appl. Phys.* **1997**, *35*, 699–708.
4. Husain, A.M. *A Small-Angle X-ray Scattering Spectrometer Utilizing an Imaging Plate Detector System. Caracterization and Implementation*; Department of Physics Technical University of Denmark: Kongens, Denmark, 1995; pp. 8–15.
5. Doyama, M.; Terashima, Y.; Ozaki, A.; Iwamoto, A.; Kanazawa, I.; Komori, F.; Eto, M. Imaging plates as position-sensitive detectors of positrons studied by the slow positron beam. *Appl. Surf. Sci.* **1999**, *149*, 71–76. [CrossRef]
6. Kobayashi, H.; Satoh, M.; Matsubyashi, M. Study for a novel tomography technique using an imaging plate. *Nucl. Instrum. Meth. A* **1999**, *424*, 221–228. [CrossRef]
7. Kobayashi, H.; Satoh, M. Basic performance of a neutron sensitive photostimulated luminescence device for neutron radiography. *Nucl. Instrum. Meth. A* **1999**, *424*, 1–8. [CrossRef]
8. Kolbe, H.; Lehmann, E.; Gunia, W.; Komer, S. Applications and characteristics of imaging plates as detector in neutron radiography at SINQ. *Nucl. Instrum. Meth. A* **1999**, *424*, 40–47. [CrossRef]
9. Wilkinson, C.; Gabriel, A.; Lehmann, M.S.; Zemb, T.; Ne, F. Image plate neutron detector. In Proceedings of the SPIE 1737, Neutrons, X Rays, and Gamma Rays: Imaging Detectors, Material Characterization Techniques, and Applications, San Diego, CA, USA, 2 February 1993. [CrossRef]

10. Niimura, N.; Karasawa, Y.; Tanaka, I.; Miyahara, J.; Takahashi, K.; Saito, H.; Koizumi, S.; Hidaka, M. An imaging plate neutron detector. *Nucl. Instrum. Meth. A* **1994**, *349*, 521–525. [CrossRef]
11. Cipriani, F.; Castagna, J.-C.; Claustre, L.; Wilkinson, C.; Lehmann, M.S. Large area neutron and X-ray image-plate detectors for macromolecular biology. *Nucl. Instrum. Meth. A* **1997**, *392*, 471–474. [CrossRef]
12. Wilkinson, C.; Cowan, J.A.; Myles, D.A.A.; Cipriani, F.; McIntyre, G.J. VIVALDI—A thermal-neutron laue diffractometer for physics, chemistry and materials science. *Neutron News* **2002**, *13*, 37–41. [CrossRef]
13. Tosaki, M.; Nakamura, M.; Hirose, M.; Matsumoto, H. Application of heavy-ion microbeam system at Kyoto University: Energy response for imaging plate by single ion irradiation. *Nucl. Instrum. Meth. B* **2011**, *269*, 3145–3148. [CrossRef]
14. Batentschuk, M.; Winnacker, A.; Schwartz, K.; Trautmann, C. Storage efficiency of BaFBr:Eu^{2+} image plates irradiated by swift heavy ions. *J. Lumin.* **2007**, *125*, 40–44. [CrossRef]
15. Beck, H.P. A study on mixed halide compounds MFX (M = Ca, Sr, Eu, Ba; X = Cl, Br, I). *J. Solid State Chem.* **1976**, *17*, 275–282. [CrossRef]
16. Nicollin, D.; Bill, H. Experimental contribution to the study of S-state ions in ionic single crystals. *J. Phys. C Solid State* **1978**, *11*, 4803–4814. [CrossRef]
17. Zimmermann, J.; Kolb, R.; Hesse, S.; Schlapp, M.; Schmechel, R.; von Seggern, H. Preparation-induced F-centre transformation in BaFBr:Eu^{2+}. *J. Phys. D Appl. Phys.* **2004**, *37*, 2352. [CrossRef]
18. Koschnick, F.K.; Spaeth, J.M.; Eachus, R.S.; McDugle, W.G.; Nuttall, R.H.D. Experimental evidence for the aggregation of photostimulable centers in BaFBr:Eu^{2+} single crystals by cross relaxation spectroscopy. *Phys. Rev. Lett.* **1991**, *67*, 3571. [CrossRef] [PubMed]
19. Takahashi, K. Progress in science and technology on photostimulable BaFX:Eu^{2+} (X = Cl, Br, I) and imaging plates. *J. Lumin.* **2002**, *100*, 307–315. [CrossRef]
20. Spaeth, J.M. Recent developments in X-ray storage phosphor materials. *Radiat. Meas.* **2001**, *33*, 527–532. [CrossRef]
21. Spaeth, J.M.; Hangleiter, T.; Koschnick, F.K.; Pawlik, T. X-ray storage phosphors. *Radiat. Eff. Defect S.* **1995**, *135*, 1–10. [CrossRef]
22. Hall, C.; Kamenskikh, I.A.; Gurvich, A.M.; Munro, I.H.; Mikhailin, V.V.; Worgan, J.S. Phosphors for Luminescent Image Plates. *J. X-ray Sci. Technol.* **1996**, *6*, 48–62. [CrossRef]
23. Nanto, H.; Okada, G. Optically stimulated luminescence dosimeters: Principles, phosphors and applications. *Jpn. J. Appl. Phys.* **2022**, *62*, 010505. [CrossRef]
24. Popov, A.I.; Kotomin, E.A.; Maier, J. Analysis of self-trapped hole mobility in alkali halides and metal halides. *Solid State Ion.* **2017**, *302*, 3–6. [CrossRef]
25. Sidorenko, A.V.; Bos, A.J.J.; Dorenbos, P.; Van Eijk, C.W.E.; Rodnyi, P.A.; Berezovskaya, I.V.; Popov, A.I. Storage properties of Ce^{3+} doped haloborate phosphors enriched with ^{10}B isotope. *J. Appl. Phys.* **2004**, *95*, 7898–7902. [CrossRef]
26. Harrison, A.; Lane, L.C.; Templer, R.H.; Seddon, J.M. Mechanism of charge storage and luminescence stimulation in BaFBr: RE phosphors. *Nucl. Instrum. Meth. A* **1991**, *310*, 220–223. [CrossRef]
27. Zhao, W.; Mi, Y.M.; Song, Z.F.; Su, M.Z. Color Centers in the Near Infrared Region in Crystals MFX (M = Ba, Sr; X = Cl, Br). *J. Solid State Chem.* **1993**, *103*, 415–419. [CrossRef]
28. Kurobori, T.K.T.; Kawabe, M.K.M.; Liu, M.L.M.; Hirose, Y.H.Y. Experimental evidence for the aggregation of the near-IR bands in BaFBr: Eu^{2+} single crystals. *Jpn. J. Appl. Phys.* **2000**, *39*, L629–L632. [CrossRef]
29. Hangleiter, T.; Koschnick, F.K.; Spaeth, J.M.; Eachus, R.S. Photo-stimulated emission of X-irradiated BaFBr:Eu. *Radiat. Eff. Defects Solids* **1991**, *119–121*, 615–620. [CrossRef]
30. Bradford, M.; Andrews, D.A.; Harrison, A.; Roden, S.G.; King, T.K. Photostimulated luminescence of BaFBr: Eu^{2+}. *J. Lumin.* **1997**, *72*, 742–744. [CrossRef]
31. Chen, W.S.; Mianzeng, L. Photostimulated luminescence of BaFBr.Eu phosphors. *J. Appl. Phys.* **1996**, *80*, 5309–5311. [CrossRef]
32. Fong, F.K.; Yocom, P.N. Crystal growth and color center of alkaline-earth halides. *J. Chem. Phys.* **1964**, *41*, 1383–1388. [CrossRef]
33. Nicklaus, E.; Fisher, Y.A. modified Kiropulus method for growing BaFCl single crystals. *J. Cryst. Growth* **1972**, *12*, 337–338. [CrossRef]
34. Starick, D.; Gurvich, A.M.; Myagkova, M.G.; Rudiger, J.; Herzog, G. The Influence of Preparation Conditions on the Performance of BaFBr-Eu Storage Phosphors. *Nucl. Tracks Rad. Meas.* **1993**, *21*, 39–41. [CrossRef]
35. Ziegler, J.F.; Ziegler, M.D.; Biersak, J.P. SRIM—The stopping and range of ions in matter. *Nucl. Instrum. Methods Phys. Res. Sect. B* **2010**, *268*, 1818–1823. [CrossRef]
36. Koschnick, F.K.; Hangleiter, T.; Song, K.S.; Spaeth, J.M. Optically detected magnetic resonance study of an oxygen-vacancy complex in BaFBr. *J. Phys. Condens. Matter* **1995**, *7*, 6925–6937. [CrossRef]
37. Eachus, R.S.; McDugle, W.G.; Nuttal, R.H.D.; Olm, M.T.; Koschnick, F.K.; Hangleiter, T.; Spaeth, J.-M. Radiation-produced electron and hole centres in oxygen-containing BaFBr. I. EPR and ODEPR studies. *J. Phys. Condens. Matter* **1991**, *3*, 9327. [CrossRef]
38. Eachus, R.S.; McDugle, W.G.; Nuttal, R.H.D.; Olm, M.T.; Koschnick, F.K.; Hangleiter, T.; Spaeth, J.-M. Radiation-produced electron and hole centres in oxygen-containing BaFBr. II. An ENDOR study of O_F^-. *J. Phys. Condens. Matter* **1991**, *3*, 9339. [CrossRef]
39. Schweizer, S.; Spaeth, J.-M. New oxygen hole centres in the X-ray storage phosphor BaFBr. *J. Phys. Condens. Matter* **1999**, *11*, 1723. [CrossRef]
40. Schweizer, S. Physics and Current Understanding of X-ray Storage Phosphors. *Phys. Stat. Sol. (A)* **2001**, *182*, 335–393. [CrossRef]

41. Radzhabov, E.; Otroshok, V. Optical spectra of oxygen defects in BaFCl and BaFBr crystals. *J. Phys. Chem. Solids* **1995**, *56*, 1–7. [CrossRef]
42. von Seggern, H. Photostimulable X-ray storage phosphors: A review of present understanding. *Braz. J. Phys.* **1999**, *29*, 254–268. [CrossRef]
43. Chadderton, L.T.; Montagu–Pollock, H.M. Fission fragment damage to crystal lattices: Heat-sensitive crystals. *Proc. R. Soc. London. Ser. A. Math. Phys. Sci.* **1963**, *274*, 239–252. [CrossRef]
44. Aumayr, F.; Facsko, S.; El-Said, A.S.; Trautmann, C.; Schleberger, M. Single ion induced surface nanostructures: A comparison between slow highly charged and swift heavy ions. *J. Phys. Condens. Matter.* **2011**, *23*, 393001. [CrossRef]
45. Trautmann, C.; Schwartz, K.; Costantini, J.M.; Steckenreiter, T.; Toulemonde, M. Radiation defects in lithium fluoride induced by heavy ions. *Nucl. Instr. Meth. B.* **1998**, *146*, 367–378. [CrossRef]
46. Toulemonde, M.; Assmann, W.; Trautmann, C.; Gruner, F. Jetlike Component in Sputtering of LiF Induced by Swift Heavy Ions. *Phys. Rev. Lett.* **2001**, *88*, 0576021. [CrossRef] [PubMed]
47. Muller, C.; Cranney, M.; El-Said, A.; Ishikawa, N.; Iwase, A.; Lang, M.; Neumann, R. Ion tracks on LiF and CaF_2 single crystals characterized by scanning force microscopy. *Nucl. Instr. and Meth. B.* **2002**, *191*, 246. [CrossRef]
48. O'Connell, J.H.; Aralbayeva, G.; Skuratov, V.A.; Saifulin, M.; Janse van Vuuren, A.; Akilbekov, A.; Zdorovets, M. Temperature dependence of swift heavy ion irradiation induced hillocks in TiO_2. *Mater. Res. Express* **2018**, *5*, 055015. [CrossRef]
49. Ishikawa, N.; Taguchi, T.; Okubo, N. Hillocks created for amorphizable and nonamorphizable ceramics irradiated with swift heavy ions: TEM study. *Nanotechnology* **2017**, *28*, 445708. [CrossRef] [PubMed]
50. Tuschel, D. Raman Spectroscopy and Chemical Bonding of BaFCl, BaFBr, and BaFl. *Spectroscopy* **2021**, *36*, 7–10. [CrossRef]
51. Scott, J.F. Raman Spectra of BaClF, BaBrF, and SrClF. *J. Chem. Phys.* **1968**, *49*, 2766–2769. [CrossRef]
52. Haeuseler, H. Lattice dynamics of BaFBr. *Phys. Chem. Mater.* **1981**, *7*, 135–137. [CrossRef]
53. Akilbekov, A.; Kenbayev, D.; Dauletbekova, A.; Polisadova, E.; Yakovlev, V.; Karipbayev, Z.; Shalaev, A.; Elsts, E.; Popov, A.I. The Effect of Fast Kr Ion Irradiation on the Optical Absorption, Luminescence, and Raman Spectra of BaFBr Crystals. *Crystals* **2023**, *13*, 1260. [CrossRef]
54. Rzepka, E.; Doualan, J.L.; Lefrant, S.; Taurel, L. Raman scattering induced by V centres in KBr. *J. Phys. C Solid State Phys.* **1982**, *15*, L119–L123. [CrossRef]
55. Akilbekov, A.; Dauletbekova, A.; Elango, A. Photo-and Thermochemical Reactions with Participation of $Br-$ Centres in X-Rayed KBr. *Phys. Stat. Sol. (B)* **1985**, *127*, 493–501. [CrossRef]
56. Rutter, H.H.; von Seggern, H.; Reininger, R.; Saile, V. Creation of Photostimulable Centers in BaFBr-Eu Single Crystals by Vacuum-ultraviolet radiation. *Phys. Rev. Lett.* **1990**, *65*, 2438–2441. [CrossRef]

Tthe Institute of Solid State Physics, University of Latvia, as the Center of Excellence has received funding from the European Union's Horizon 2020 Framework Program H2020-WIDESPREAD-01-2016-2017-TeamingPhase2 under grant agreement No. 739508, project CAMART2.